The Behavior of the Ru-bda Water Oxidation Catalysts at Low Oxidation States

Roc Matheu,[a] Abolfazl Ghaderian,[a] Laia Francàs,[a] Petko Chernev,[b] Mehmed Z. Ertem,[c] Jordi Benet-Buchholz,[a] Victor Batista,[d,*] Michael Haumann,[b] Carolina Gimbert-Suriñach,[a,*] Xavier Sala,[e,*] and Antoni Llobet[a,e,*]

[a] Institute of Chemical Research of Catalonia (ICIQ), Barcelona Institute of Technology (BIST), Avinguda Països Catalans 16, 43007 Tarragona, Spain.

[b] Institute for Experimental Physics, Free University Berlin, D-14195 Berlin, Germany.

[c] Chemistry Department, Brookhaven National Laboratory, Upton, NY 11973, USA.

[d] Department of Chemistry, Yale University. P.O. Box 208107, New Haven, CT 06520-8107, USA.

[e] Departament de Química, Universitat Autònoma de Barcelona, Cerdanyola del Vallès, 08193 Barcelona, Spain.

Corresponding authors: cgimbert@iciq.es; victor.batista@yale.edu; xavier.sala@uab.cat; allobet@iciq.es.

Abstract

The Ru complex $[Ru^{II}(bda\text{-}\kappa\text{-}N^2O^2)(N\text{-}NH_2)_2]$, **1**, ($bda^{2-}$ = (2,2'-bipyridine)-6,6'-dicarboxylate; $N\text{-}NH_2$ = 4-(pyridin-4-yl)aniline) is used as a synthetic intermediate to prepare new Ru-bda complexes that contain the NO^+, acetonitrile (MeCN) or H_2O ligands at oxidation states II and III. Complex **1** in acidic solutions reacts with excess NO^+ (generated *in situ* from sodium nitrite) to form a new Ru complex where the aryl amines ligand $N\text{-}NH_2$ in **1** are transformed into diazonium salts ($N\text{-}N_2^+$ = 4-(pyridin-4-yl)benzenediazonium)) together with the formation of a new Ru-NO group at the equatorial zone, to generate $[Ru^{II}(bda\text{-}\kappa\text{-}N^2O)(NO)(N\text{-}N_2)_2]^{3+}$, $\mathbf{2}^{3+}$. Here the bda ligand only acts in a tridentate manner as $\kappa\text{-}N^2O$ with a dangling carboxylato group. Similarly complex **1** can also react with a coordinating solvent, such as MeCN, at room temperature leading to complex $[Ru^{II}(bda\text{-}\kappa\text{-}N^2O)(MeCN)(N\text{-}NH_2)_2]$, **3**. Finally in acidic aqueous solutions a related reaction occurs where solvent water coordinates the Ru center forming $\{[Ru^{II}(bda\text{-}\kappa\text{-}(NO)^3)(H_2O)(N\text{-}NH_3)_2](H_2O)_n\}^{2+}$, $\mathbf{4}^{2+}$, that is strongly hydrogen bonded with additional water molecules at the second coordination sphere. Furthermore, under acidic conditions the aniline ligands are also protonated forming the corresponding anilinium cationic ligands $N\text{-}NH_3^+$. We have additionally characterized the one electron oxidized complex $\{[Ru^{III}(bda\text{-}\kappa\text{-}(NO)^{3.5})(H_2O)(N\text{-}NH_3)_2](H_2O)_n\}^{3+}$, $\mathbf{5}^{3+}$. The fractional value of κ notation, indicates the presence of an additional contact to the pseudo-octahedral geometry of the Ru metal center. The coordination mode of the complexes has been studied both in the solid state and in solution through single-crystal X-ray diffraction, X-ray absorption spectroscopy, variable-temperature NMR and density functional theory calculations. While the $\kappa\text{-}N^2O$ is the main coordination mode for $\mathbf{2}^{3+}$ and **3**, an equilibrium that involves isomers with $\kappa\text{-}N^2O$ and $\kappa\text{-}NO^2$ coordination modes and neighboring hydrogen bonded water molecules is observed for $\mathbf{4}^{2+}$ and $\mathbf{5}^{3+}$.

Keywords

water oxidation catalysis, water splitting, Ru complexes, water coordination, frustrated coordination site, Ru-bda complexes

1. Introduction

The field of water oxidation catalysis (WOC) by molecular transition metal complexes has evolved enormously since the early work of Meyer and co-workers on the blue dimer[1] back in the early eighties up to now.[2] Extremely rugged molecular WOCs based on Ru complexes with turnover numbers (TON) in some cases over a million have been recently reported with confirmed molecular structure maintained over the entire catalytic performance.[3,4,5] A prominent family of these catalysts are Ru complexes based on the tetradentate ligand 2,2'-bipyridine-6,6'-dicarboxylato (bda^{2-}; see Chart 1 for a drawing of all the ligands described in this work), named Ru-bda type of complexes that have been recently reported.[6,7,8,9,10] In some cases these complexes have catalytic activity that is comparable to that of the natural oxygen evolving complex of photosystem II (OEC-PSII) in green plants and algae.[11,12] Further, even faster catalysts have been reported recently containing a related pentadentate ligand, such as 2,2':6',2"-terpyridine-6,6"-dicarboxylate (tda^{2-}, see Chart 1).[13,14]

The Ru-bda complexes of general formula $[Ru(bda)(N\text{-}Ax)_2]$ (N-Ax is a neutral monodentate pyridyl type of ligand in axial position) constitute a family of complexes that are easy to prepare and whose properties can be nicely tuned through the axial ligand. Indeed, the different nature of the axial ligand can exert steric, electronic or supramolecular effects that influence the properties of the catalyst.[2,6,8,15,16] In addition, axial ligands with the adequate functionalities have been used to immobilize this class of complexes on conducting solid surfaces.[17,18,19,20,21]

At oxidation state II the $[Ru(bda)(N\text{-}Ax)_2]$ complexes have a saturated coordination sphere with a distorted octahedral type of symmetry. As such they are not water oxidation catalysts but actually catalyst precursors. Those complexes enter the catalytic cycle upon coordinating a water molecule and reaching higher oxidation states.[6,20,22,23] The Ru-aqua functionality is important since it provides the capacity to loose protons and electrons in a concerted fashion at relatively low potentials and at the same time provides for a O-O bond formation site. For the particular case where the axial ligand is 4-Methylpyridine (4-Me-py), an X-ray crystal structure of $\{[[Ru^{IV}(OH)(bda\text{-}\kappa\text{-}N^2O^2)(4\text{-}Me\text{-}py)_2](H_2O)]_2(\mu\text{-}H)\}^{3+}$ reveals a *seven coordinate* sphere for the Ru(IV) metal center in a pseudo pentagonal-bipyramid geometry.[24] In sharp contrast, at oxidation state II, the corresponding Ru-aqua complexes are not well characterized. Interestingly, the coordination geometry of the d^6 Ru(II) ion is expected to be octahedral since a seven coordination would imply the violation of the 18 electron rule.[25] Thus, assuming the axial ligands do not detach from the Ru-aqua complex, as evidenced by ^{1}H-NMR spectroscopy,[23] the bda^{2-} ligand must partially decoordinate to generate either a dangling carboxylate or a frustrated coordination site via decoordination of one of Ru-N bonds of the bda^{2-} bipyridyl moiety.[20,23,26] The latter is an interesting concept, recently developed, with implications in a variety of processes including heterolytic H_2 splitting. [27,28]

The main goal of the present work is to shed light on the potential coordination modes of the bda^{2-} ligand at low oxidation states (*i.e.,* Ru(II) and Ru(III)) which is crucial for the aqua ligand coordination that provides the entry into the catalytic cycle. For this purpose, we have prepared a family of Ru-

bda complexes (see complexes **1**-**5**$^{3+}$ in Scheme 1) and characterized them by x-ray diffraction and spectroscopic methods as well as by density functional theory (DFT) calculations.

2. Results and Discussion

2.1 Synthesis and solid state structure

We use complex [Ru^{II}(bda-κ-N^2O^2)(N-NH_2)$_2$], **1**,[17] that contains 4-(pyridin-4-yl)aniline (N-NH_2) ligands at axial positions, as the starting material for all the complexes described in this work, following the synthetic strategy depicted in Scheme 1. In this work we selected **1** because of its solubility both in organic solvents and acidic water and because the amino functionality gives an easy synthetic access to the family of Ru-bda complexes depicted in Scheme 1. This family allows to obtain a large variety of spectroscopic properties that analyzed together provide a consistent and comprehensive description of the phenomena occurring in Ru-bda complexes at low oxidation sates. Further, the remote situation of the amino groups doesn't influence significantly the redox potential of the Ru complex.[17]

The solid-state structure of **1** was analyzed by X-ray diffraction (XRD), Density functional theory (DFT) calculations and X-ray absorption spectroscopy (XAS). Monocrystals of **1** were obtained by slow diffusion of diethyl ether into a methanol solution and an ORTEP drawing of its structure is shown in Figure 1. The bonding distances and angles found in this structure are similar to related Ru(II) complexes containing similar type of ligands ($d_{Ru-O/Ru-N}$ = 1.9 - 2.1 Å).[24,29,30,31] The most interesting feature is the equatorial geometry of the first coordination sphere imposed by the bda^{2-} ligand, generating an ORuO angle of 121.7°. XAS at the Ru K-edge was carried on a powder of **1**, and the results are reported in Figure 2. The bonding distances obtained by Extended X-ray absorption fine structure (EXAFS) simulation are presented in Table 1 and show very good agreement with the XRD data. Further, DFT calculations were carried out for the geometrical optimization of **1** at the M06 level of theory[32] and the main geometric parameters are also displayed in Table 1, whereas the complete data can be found in the Supporting Information (SI). It is worth noting here the high degree of consistency of all the metric parameters obtained for **1** by these three methodologies bringing a good degree of confidence when used for other related structural characterizations that will be discussed further on.

Complex **1** reacts with excess NO^+ in acid (generated *in situ* from sodium nitrite) [33] to form complex [Ru^{II}(bda-κ-N^2O)(NO)(N-N_2)$_2$]$^{3+}$, **2**$^{3+}$, where the aryl amines of **1** are transformed into diazonium salts (N-N_2^+ = is 4-(pyridin-4-yl)benzenediazonium)). In addition, a new Ru-NO group is also formed at the equatorial zone according to equation 1. Addition of a saturated solution of KPF_6 allows its isolation as a powdery salt.[17]

$$[Ru^{II}(bda\text{-}\kappa\text{-}N^2O^2)(N\text{-}NH_2)_2] + 3\ NO^+ \rightarrow [Ru^{II}(bda\text{-}\kappa\text{-}N^2O)(NO)(N\text{-}N_2)_2]^{3+} + 2\ H_2O \quad (1)$$

1 **2**$^{3+}$

Suitable single crystals for x-ray diffraction analysis of $\mathbf{2}^{3+}$ were obtained by slow evaporation of an acidic aqueous solution of $\mathbf{2}^{3+}$. Figure 1 shows the ORTEP representation where the nitrosyl group occupies one of the equatorial positions, while the bda^{2-} exhibits κ-N^2O coordination mode. Such coordination mode releases the geometrical strain in the equatorial plane described in **1**, and produces a dangling carboxylate not bonded to the Ru metal center. The κ-N^2O coordination mode is also favored by the crystal packing of the molecule where the dangling carboxylate interacts with the N atoms of the diazonium groups of another molecule, forming dimers as shown with green dashes in Figure S9. With regard to the Ru-NO^+ group, the near linearity of the Ru-N-O^+ bond (175.8°) and the N-O bond length (d_{N-O} = 1.13 Å) indicate a N-O triple bond character. The DFT calculations at the M06 level again gives geometric parameters that are very consistent with those obtained by X-ray diffraction as can be seen in Figure 3 left and Table S2. In particular, $\mathbf{2}^{3+}$ is assigned as closed-shell singlet with a near lineal Ru-N-O^+ bond (174.7 °) and d_{N-O} = 1.14 Å confirming the Ru^{II}-($N\equiv O^+$) nature.

Complex **1** can also react with a coordinating solvent, such as MeCN at room temperature, leading to complex $[Ru^{II}(bda\text{-}\kappa\text{-}N^2O)(MeCN)(N\text{-}NH_2)_2]$, **3**, as shown in equation 2. In this complex, the MeCN coordinates the Ru center in the equatorial plane and again forces the Ru-bda moiety to rearrange its coordination mode by releasing one carboxylate, similar to what is observed for $\mathbf{2}^{3+}$. Single crystals of **3** were obtained by slow diffusion of diethyl ether to a 4:1 MeOH:MeCN solution of **1**, and its ORTEP plot is exhibited in Figure 1. The bda^{2-} ligand coordinates the Ru center in a κ-N^2O fashion with a pendant carboxylate similar to the coordination mode exhibited by $\mathbf{2}^{3+}$. Here again the computational calculations at the M06 level provided geometric parameters for **3** analogous to those obtained by means of XRD (see Table S3)

$$\underset{\mathbf{1}}{[Ru^{II}(bda\text{-}\kappa\text{-}N^2O^2)(N\text{-}NH_2)_2]} + MeCN \rightleftharpoons \underset{\mathbf{3}}{[Ru^{II}(bda\text{-}\kappa\text{-}N^2O)(MeCN)(N\text{-}NH_2)_2]} \qquad (2)$$

The coordination of MeCN is subject to an equilibrium where the solvent molecule coordinates and decoordinates the Ru center. This equilibrium can be controlled by the concentration of MeCN solvent. For instance, the addition of a 20% of MeCN to a methanol solution of **1** allows the quantitative generation of **3** as determined by 1D and 2D NMR spectroscopy (see Figures S1-S7). However, even if the amount of **1** present in the equilibrium is negligible, as indicated by NMR, it precipitates from the solution as a powder, probably due to its very low solubility.

At pH = 1.0, **1** reacts with the water solvent forming complex $\{[Ru^{II}(bda\text{-}\kappa\text{-}(NO)^3)(H_2O)(N\text{-}NH_3)_2](H_2O)_n\}^{2+}$, $\mathbf{4}^{2+}$, as shown in equation 3. Again, the coordination occurs at the equatorial plane with subsequent rearranging of the coordination mode of bda^{2-} ligand. In this case, the modification of the first coordination sphere involves the presence of a network of strongly hydrogen bonded

H_2O molecules as a second coordination sphere. The number of H_2O molecules involved in this network is designated as "*n*" and they are strongly interacting with the Ru-aqua group and the carboxylate moieties of the bda^{2-} ligand. In addition, the amino groups at this pH are protonated forming the corresponding ammonium salts. The proposed label $\mathbf{4^{2+}}$, represents two limit isomeric structures namely $\mathbf{[4\text{-}\kappa\text{-}N^2O(H_2O)_n]^{2+}}$ and $\mathbf{[4\text{-}\kappa\text{-}NO^2(H_2O)_n]^{2+}}$, (denoted as κ-$(NO)^3$) whose relative occurrence will be discussed in the following sections. As observed for **3**, in the solid state the equilibrium shifts towards the more insoluble isomer generating **1** again with no water coordinated at the metal center.

$$[Ru^{II}(bda\text{-}\kappa\text{-}N^2O^2)(N\text{-}NH_2)_2] + 2H^+ + (n+1)\,H_2O \rightleftharpoons \{[Ru^{II}(bda\text{-}\kappa\text{-}(NO)^3)(H_2O)(N\text{-}NH_3)_2](H_2O)_n\}^{2+} \quad (3)$$

1 $\qquad$ **4^{2+}**

Finally, $\mathbf{4^{2+}}$ can easily be oxidized by atmospheric oxygen to the paramagnetic d^5 Ru(III) complex $\{[Ru^{III}(bda\text{-}\kappa\text{-}(NO)^{3.5}(H_2O)(N\text{-}NH_3)_2](H_2O)_n\}^{2+}$, $\mathbf{5^{3+}}$, as presented in Scheme 1. The fractional value of κ notation here indicates the presence of an additional contact to the pseudo-octahedral geometry of the Ru metal center at we consistently found for these type of complexes. This oxidation has been monitored by UV-vis spectroscopy and takes place with a $t_{1/2}$ of approximately 3.3 minutes at RT according to a first order mechanism (see Figures S10-S11). The complex has been analyzed in solution by Electron Paramagnetic Resonance (EPR) and XAS as it will be described in the following sections and in the SI.

2.2. Dynamic behavior in organic solvents

The solution structure of $\mathbf{2^{3+}}$ and **3** were investigated by VT-NMR in organic solvents and by DFT calculations and the spectra are shown in Figure 4 and in Figures S12-S13. Figure 4 shows the ^{1}H-NMR spectra of $\mathbf{2^{3+}}$ in acetone-d_6 in the temperature range 273-193 K. At 273 K the ^{1}H-NMR spectrum of $\mathbf{2}^{3+}$ is not consistent with the κ-N^2O binding mode of the bda^{2-} ligand displayed in the solid state X-ray structure. As the temperature is lowered the resonances due to the bda^{2-} ligand broaden and split, now consistent with the asymmetry observed in the X-ray structure. At 193 K all the resonances are unambiguously assigned based on 2D-NMR spectroscopy (see Figure S12) and in agreement with the DFT calculated chemical shifts (see Figure 4). The broadening and splitting of the bda^{2-} resonances at lower temperatures points out to the presence of dynamic behavior where the two carboxylates of the bda^{2-} ligand coordinate and decoordinate very fast as graphically shown in Scheme 2. This is further corroborated by the fact that the resonances for protons C and C' contiguous to the carboxylate group, are by far the ones that suffer the largest shift of more than 0.4 ppm (see Chart 1). An energy of activation of 12.5 kcal/mol is obtained for this process from the spectra (see Figure S14). We also obtained optimized structures for Ru^{II}-NO^+ complexes via DFT calculations in both κ-N^2O and κ-$(NO)^3$ modes of bda^{2-} ligand and found the latter binding mode,

that is proposed to be the transition state in the interconversion, to be higher in energy by 6.2 kcal/mol (see Scheme 2 and Figure 3).

A similar behavior is observed for the Ru^{II}-MeCN complex **3** dissolved in a 1:4 acetonitrile-d_3:methanol-d_4 mixture but with subtle differences (see Figure S13)**.** At room temperature the main isomer observed is the κ-N^2O that upon heating to temperature close to 320 K, its resonances coalesce. In this case, the energy of activation obtained from the spectra is 15.0 kcal/mol (see Figure S15).

The X-ray structures and VT-NMR results, just described, clearly show the preference for a κ-N^2O coordination mode for the bda^{2-} ligand in $\mathbf{2}^{3+}$ and **3**, in the absence of as second coordination sphere hydrogen bonding. The preference for the κ-N^2O coordination mode for Ru-bda complexes coordinating the MeCN ligand has been observed in related Ru-bda complexes[,34,35] This is in agreement with the HSAB theory,[36] where Ru at low oxidation states prefers soft π-acceptor ligands such as N-pyridyl over hard O-carboxylate ligands.

2.3. Dynamic behavior in acidic aqueous solutions

The ^{1}H-NMR spectrum of **1** was recorded in methanol-d_4 at room temperature and with increasing amounts of a pD = 1.0 solution as indicated in the spectra shown in Figure 5. In pure methanol-d_4 the ^{1}H-NMR spectrum of **1** shows the typical behavior of a six coordinated Ru(II) complex with C_{2v} symmetry. All resonances could be unambiguously assigned based on 2D NMR spectra[17] and also supported by computed NMR chemical shifts at M06 level of theory. However, the addition of CF_3SO_3D dissolved in D_2O, significantly broaden resonances and some of them are strongly shifted as observed in Figure 5. The F labelled protons (Chart I), which are close to the amino group, suffer the highest shift due to the protonation of the amino group. The small shift of the D protons indicates that the Ru center is almost unaffected by the protonation of the amines. Further, at 25% of pD = 1.0 solution, we carried out VT-NMR all the way to 240 K where the resonances sharpen again, as shown in Figure 5 (right), consistent with the presence of a single symmetrical isomer. In contrast to the previous VT-NMR spectra for $\mathbf{2}^{3+}$, now both B and C protons are similarly shifted which advocates for a different type of dynamic behavior where both the Ru-N and Ru-O bonds are simultaneously being formed and broken as proposed in Scheme 3. Further, the VT-NMR results are consistent with the coordination of a water molecule to the Ru metal center upon addition of an acidic aqueous solution. The formation and braking of the Ru(II)-OH_2 bond occurs simultaneously with a dynamic behavior involving species $\mathbf{[4\text{-}\kappa\text{-}N^2O(H_2O)_n]^{2+}}$ and $\mathbf{[4\text{-}\kappa\text{-}NO^2(H_2O)_n]^{2+}}$, that interconvert through the transition states TS-A, TS-B and TS-C (Scheme 3). The sharpening at low temperature of the ^{1}H resonances is consistent the absence of the coordination/decoordination of water to the Ru center but with all the equilibria indicated in Scheme 3 occurring very fast. In sharp contrast, when **1** is dissolved in neutral aqueous solutions, methanol-d_4:D_2O (4:1), the VT ^{1}H-NMR experiment reveals that the aqua coordination/decoordination to Ru equilibrium is still present (Figure S16).

The presence of the **[4-κ-NO^2(H$_2$O)$_n$]$^{2+}$** species is favored by solvent H_2O molecules strongly hydrogen bonded to the Ru-H_2O group and the carboxylato moiety of the bda^{2-} ligand. This hydrogen bonding will push the bpy part of the bda^{2-} ligand away from the metal center and explains why the intuitively preferred Ru-N coordination mode for a soft low spin d^6 Ru(II) ion is not always favored.

All the NMR measurements were performed under strict N_2 conditions to avoid the oxidation of **4^{2+}** to **5^{3+}** (see NMR methods in the SI for further details). In order to further prove that **4^{2+}** remains at oxidation state II, we prepared solutions of **4^{2+}** identically to those prepared for NMR analysis and carried out EPR measurements. The absence of EPR signal discards the formation of any traces of the one electron oxidized species, **5^{3+}**, and thus confirms that the nature of the NMR resonance broadening is solely due to the dynamic behavior. The same behavior also occurs in other Ru-bda catalyst such as [Ru(bda-κ-N^{2}O^2)(isoq)$_2$] (isoq is isoquinoline) under exactly the same conditions as for **1**, as shown in Figure S18 in the supporting information. The comparable shift and broadening of the resonances observed for the [Ru(bda-κ-N^{2}O^2)(isoq)$_2$] complex suggests that this is a general phenomenon occurring in Ru-bda complexes.

We carried out DFT calculations for both the **[4-κ-NO^2(H$_2$O)$_n$]$^{2+}$** and **[4-κ-N^{2}O(H$_2$O)$_n$]$^{2+}$** isomers using either two or four solvated water molecules. We have chosen a limited number of water molecules as a model although it is obvious that a much larger number of water molecules will be involved as second and third coordination sphere to the Ru center. The structures with two or four solvated molecules yielded similar results in terms of geometrical features and relative energies of the isomers (see Figures S21-22 and Tables S4-S5). To simplify the discussion we present only **[4-κ-NO^2(H$_2$O)$_4$]$^{2+}$** and **[4-κ-N^{2}O(H$_2$O)$_4$]$^{2+}$** isomers and the optimized geometries and relevant metric parameters of which are depicted in Figure 6 and Table 1. The first interesting feature of the obtained optimized structures for **[4-κ-NO^2(H$_2$O)$_4$]$^{2+}$** and **[4-κ-N^{2}O(H$_2$O)$_4$]** $^{2+}$ is the presence of a hydrogen bonding network between the Ru-aqua group and the carboxylate groups of the bda^{2-} ligand that resembles the crystal structure of {[[Ru^{IV}(OH)(κ-N^{2}O^2-bda)(4-Me-py)$_2$](H$_2$O)]$_2$(μ-H)}$^{3+}$.[24] It is also interesting to compare the distances between Ru and the N and O atoms of the bda^{2-} ligand in both isomers. For the **[4-κ-N^{2}O(H$_2$O)$_4$]$^{2+}$** isomer these distances are very similar to those of **2^{3+}** with a the characteristic distance between the Ru and the O atom of the dangling carboxylate at 3.45 Å. On the other hand, for **[4-κ-NO^2(H$_2$O)$_4$]$^{2+}$**, the most unusual distances are the Ru-N that are 2.26 Å and 2.82 Å, which are 0.1 Å and 0.7 Å longer than the typical Ru-N bonds for related complexes. The computed chemical shifts at M06 level for the optimized structures (Figure S25) are not consistent with either those of the **[4-κ-N^{2}O(H$_2$O)$_4$]$^{2+}$** isomer (Path A, Scheme 3) or those of the **[4-κ-NO^2(H$_2$O)$_4$]$^{2+}$** (Path B, Scheme 3) but with a mixture of all of them. The combination of all these equilibria is depicted in Scheme 3 (Paths A, B and C), where explicit water molecules are not shown for the sake of simplicity.

The isomers of the one electron oxidized complex, **[5-κ-N^{2}O(H$_2$O)$_4$]$^{3+}$** and **[5-κ-NO^2(H$_2$O)$_4$]$^{3+}$**, were also optimized at M06 level of theory and the corresponding structures and most relevant geometric parameters are presented in Figure 6 and Table 1. For the one electron oxidized isomers, the bond distances of the first and second coordination sphere are shortened compared to those found for

the $\mathbf{4}^{2+}$ counterparts as expected.[37] However, the most relevant distances for both isomers, Ru-N of 2.46 Å for $\mathbf{[5\text{-}\kappa\text{-}NO^2(H_2O)_4]^{3+}}$ and the Ru-O distance of 3.06 Å for the dangling carboxylate in $\mathbf{[5\text{-}\kappa\text{-}N^2O(H_2O)_4]^{2+}}$ remain comparable to its related complex in the oxidation state II.

Another very interesting feature of these complexes is their relative energies. While at oxidation sate II, the $\mathbf{[4\text{-}\kappa\text{-}N^2O(H_2O)_4]^{2+}}$ isomer is favored by 20.3 kcal/mol with regard to the $\mathbf{[4\text{-}\kappa\text{-}NO^2(H_2O)_4]^{2+}}$ isomer, at oxidation state III this difference is drastically reduced to only 2.1 kcal/mol. While the energy comparison is only indicative because of the possibility of several conformers associated with solvent molecules hampering a reliable comparison, the trend is certainly significant.

In order to extract further experimental evidence about the potential combination of equilibria acting in the Ru-aqua complexes bearing the bda^{2-} ligand in aqueous solution, we carried out XAS spectroscopy of frozen solutions of $\mathbf{5}^{3+}$. The results obtained are shown in Figure 2 and Table 1 together with those of **1,** $[Ru^{III}Cl_3(trpy)]$ (trpy is 2,2':6',2"-terpyridine) and $Ru^{IV}O_2$ that were used as reference materials.

Table 1 presents the metric parameters $\mathbf{5}^{3+}$, extracted from EXAFS simulations (Figure 2B). As can be observed the EXAFS spectral changes for $\mathbf{5}^{3+}$ compared to **1** involve an overall shortening of the Ru-N/O bond lengths, leading to homogenization of the first coordination sphere of Ru-ligand distances. Very importantly a ~2.54 Å distance was detected that improves the quality of the EXAFS fit by a factor of about 2 (Table S1). This additional distance is thus indicative that the isomer $\mathbf{[5\text{-}\kappa\text{-}NO^2(H_2O)_n]^{3+}}$ is present in the mixture of isomers at this oxidation state. In addition, the metric parameters obtained from EXAFS coincide well with those obtained from the computed structures for $\mathbf{[5\text{-}\kappa\text{-}NO^2(H_2O)_4]^{3+}}$ confirming the presence of these species in frozen aqueous solution (Table 1).

To the best of our knowledge, this is the first time to experimentally demonstrate that the $\kappa\text{-}NO^2$ coordination mode for the bda^{2-} ligands is relevant in the combination of potential isomers involved in Ru-bda type of complexes at low oxidation states, although it had been suggested based on DFT calculations.[26] In addition, we also found a similar distance for the $[Ru(tda)(py)_2]$ catalyst precursor at oxidation state III, where the two isomers, $[Ru^{III}(tda\text{-}\kappa\text{-}N^2O^2)(py)_2]^+$ and $[Ru^{III}(tda\text{-}\kappa\text{-}N^3O)(py)_2]^+$, are found to coexist in the crystal structure.[13]

This counterintuitively behavior on the coordination modes of bda^{2-} in $\mathbf{4}^{2+}$ and $\mathbf{5}^{3+}$, which is different from their homologues to $\mathbf{2}^{3+}$ and **3** in organic solvents, is mainly associated with the strong hydrogen bonding belt along the aqua and carboxylato ligands. The latter provides the driving force to push away the bpy part of the bda^{2-} ligand producing a decoordination of one of the N-atoms.[26]

In summary, our results based on VT-NMR, XAS and DFT calculations provide a detailed description of the nature of the species involved in water oxidation catalysis by Ru-bda type complexes at low oxidation states, where the critical Ru-aqua group that provides access to the catalytic cycle is formed. The results show the fundamental need for a flexible and adaptable ligand, as is the case for bda^{2-}, both from an electronic and geometrical perspective, to comply with the demands of the Ru metal centers at the different oxidation states. Further, for the first time we have shown

experimentally the presence of isomers in Ru-bda type of complexes where the ligand acts in a κ-NO^2 fashion.

3. Associated content

Supporting Information (SI). Synthetic procedures; X-ray crystallographic data in CIF format (CCDC # 1014176 for **1** and 1014177 for $\mathbf{2}^{3+}$); additional experimental, spectroscopic, electrochemical and computational data.

Corresponding Authors:

victor.batista@yale.edu; xavier.sala@uab.cat; allobet@iciq.es.

5. Acknowledgments

RM, AL and XS acknowledge MINECO and FEDER (CTQ2016-80058-R, CTQ2015-64261-R, SEV 2013-0319, ENE2016-82025-REDT, CTQ2016-81923-REDC), AGAUR (2017-SGR-1631) for financial support. RM thanks "La Caixa" foundation for a PhD grant. M.H. thanks the Deutsche Forschungsgemeinschaft for financial support (grant Ha3265/6-1) and for a Heisenberg Fellowship and the German Bundesministerium für Bildung und Forschung for funding within the Röntgen-Angström Cluster (grant 05K14KE1). We thank S. Reschke and M. Görlin for help in XAS data collection and M. Nachtegaal at SuperXAS of SLS for excellent technical support. The work at Brookhaven National Laboratory (M.Z.E.) was carried out under contract DE-SC00112704 with the U.S. Department of Energy, Office of Science, Office of Basic Energy Sciences, and utilized resources at the BNL Center for Functional Nanomaterials. V.S.B. acknowledges financial support as part of the Argonne-Northwestern Solar Energy Research (ANSER) Center, an Energy Frontier Research Center funded by the U.S. Department of Energy, Office of Science, Office of Basic Energy Sciences under Award Number DE-SC0001059.

Table 1. Metric parameters obtained for **1**, $\mathbf{4}^{2+}$ and $\mathbf{5}^{3+}$ from X-ray diffraction (XRD) crystallography, EXAFS and DFT.

	1			***4*²⁺**		***5*³⁺**		
Distance[a]	XRD	EXAFS (*N*)[b]	DFT[c]	DFT[c] **[4-κ-NO²(H₂O)₄]²⁺**	DFT[c] **[4-κ-N²O(H₂O)₄]²⁺**	EXAFS (*N*)[b]	DFT[c] **[5-κ-NO²(H₂O)₄]³⁺**	DFT[c] **[5-κ-N²O(H₂O)₄]³⁺**
Ru-OH_2	--	--	--	2.09	2.18	1.92 (1)	2.03	2.13
Ru-NO	--	--	--	--	--	--	--	--
Ru-N1	1.92	1.92 (2)	1.93	**2.82**	1.94	**2.54** (1)	**2.46**	1.99
Ru-N2	1.93	…	1.93	2.26	2.12	2.11 (3)	**2.32**	2.14
Ru-O1	2.16	2.17 (2)	2.17	2.05	2.12	…	2.03	2.05
Ru-O2	2.18	...	2.17	2.23	**3.45**	…	2.08	**3.06**
Ru-N3	2.07	2.07 (2)	2.08	2.04	2.08	2.01 (2)	2.10	2.11
Ru-N4	2.09	…	2.09	2.06	2.11	…	2.10	2.14
ΔG (kcal/mol)				20.3	0.0		2.1	0.0

[a], the labeling scheme is the same as the one used for XRD data of **1** depicted in Figure 1. All distances in Å.

[b], distances between Ru and the atoms in its first and second coordination sphere. In parenthesis, *N*, is the coordination number defined as the number of atoms associated with a particular distance. Additional EXAFS fit parameters (Debye-Waller factors and error sums) are given in Table S1. N and O coordination is indistinguishable in EXAFS analysis as are the locations of ligands in equatorial or axial positions; in the table the distances from EXAFS therefore were ordered to comply with the DFT results.

[c], M06 functional, see SI for details.

[d], in bold are depicted Ru-N or Ru-O distances relevant for the κ-NO^2 *vs*. κ-N^2O isomer discussion.

Chart 1. Ligands used and discussed in this work together labels for NMR assignment.

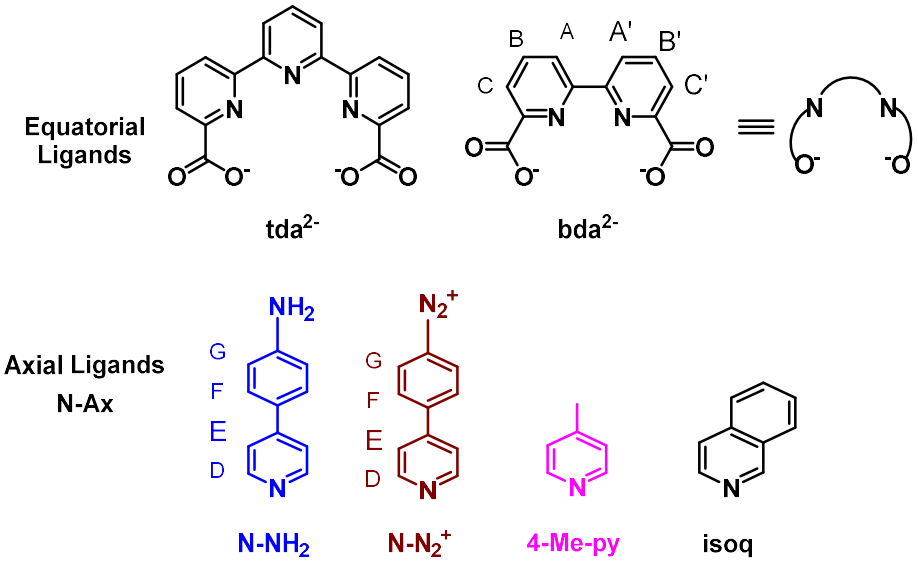

Scheme 1: General synthetic scheme and labels of complexes. The dashed lines at the first coordination sphere of the Ru metal center indicate bonds that are being simultaneously formed and broken. See Chart 1 for the detailed structure of the axial and equatorial ligands. The dashed

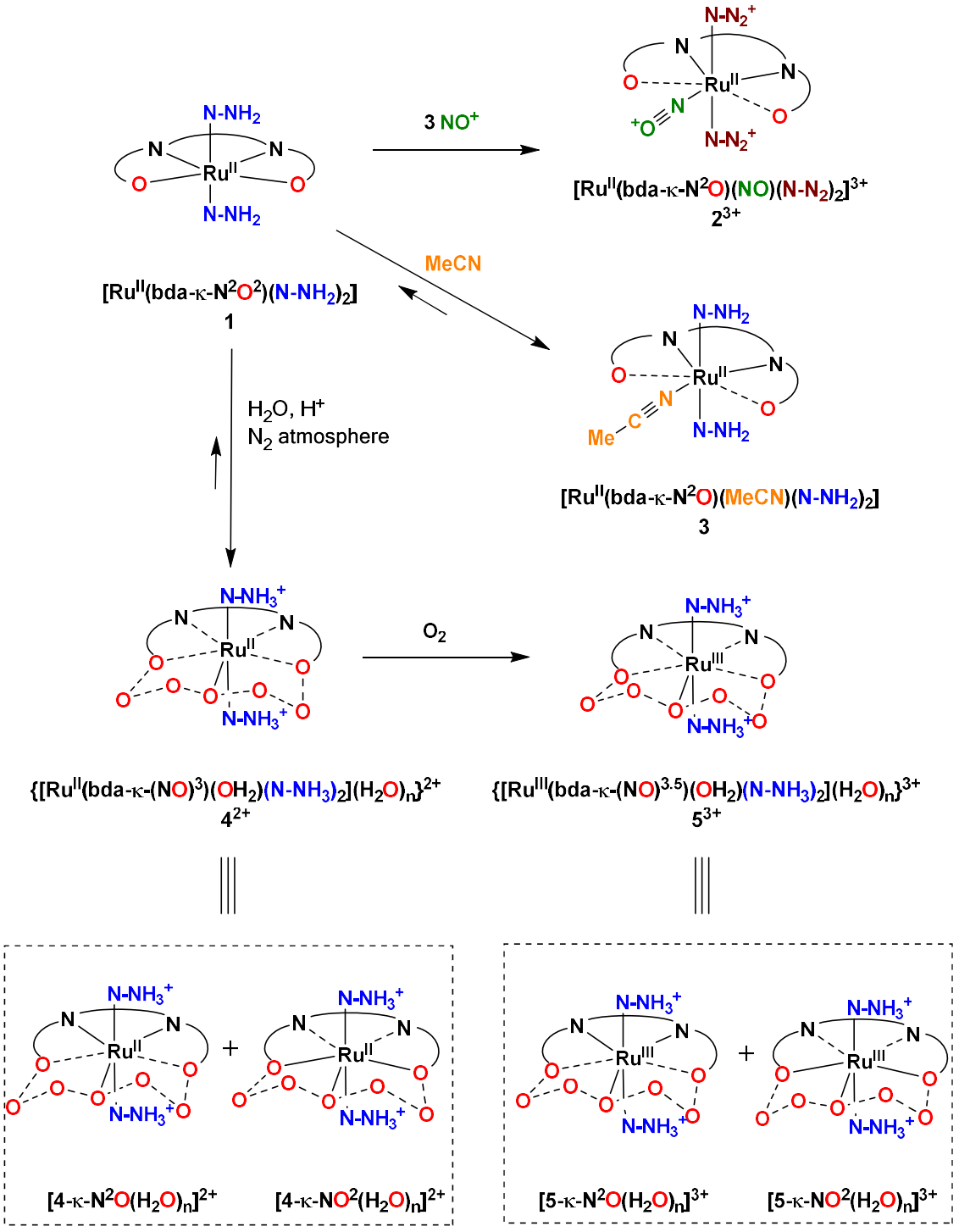

lines in $\mathbf{4}^{2+}$ and $\mathbf{5}^{3+}$ at the second coordination sphere represent hydrogen bonding from solvent water molecules

Scheme 2: Species involved in the fast equilibria associated with the dynamic behavior of $\mathbf{2}^{3+}$. Dashed lines indicate the bonds that are simultaneously formed and broken at the transition state TS-A. The DFT calculates TS structure for this complex is depicted in Figure 3 right.

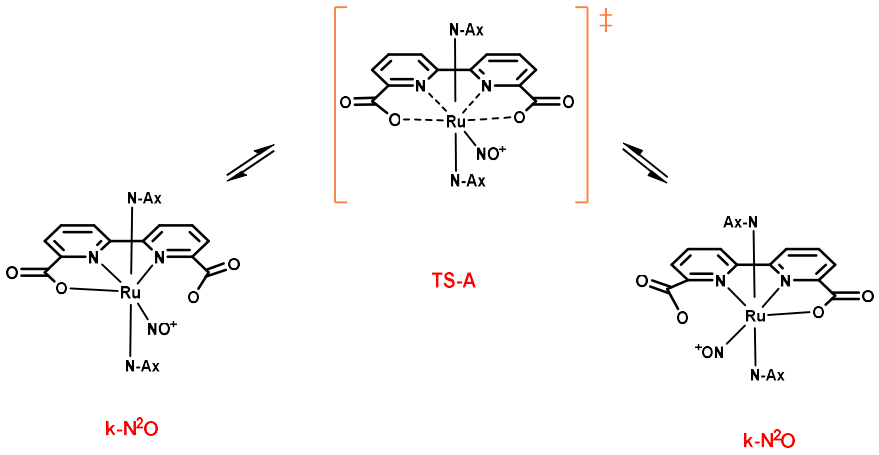

Scheme 3 Reaction pathways leading to a combination of equilibria involved in dynamic behavior of $\mathbf{4}^{2+}$ or $\mathbf{5}^{3+}$ in acidic aqueous solution. The dashed lines indicate bonds that are simultaneously formed and broken in the transition states. Water solvation molecules are not shown for clarity purposes. Three different type of pathways are identified depending on the transition state through which the species are interconverted. Thus path A involves "TS-A" whereas paths B and C involve "TS-B" and "TS-C" respectively.

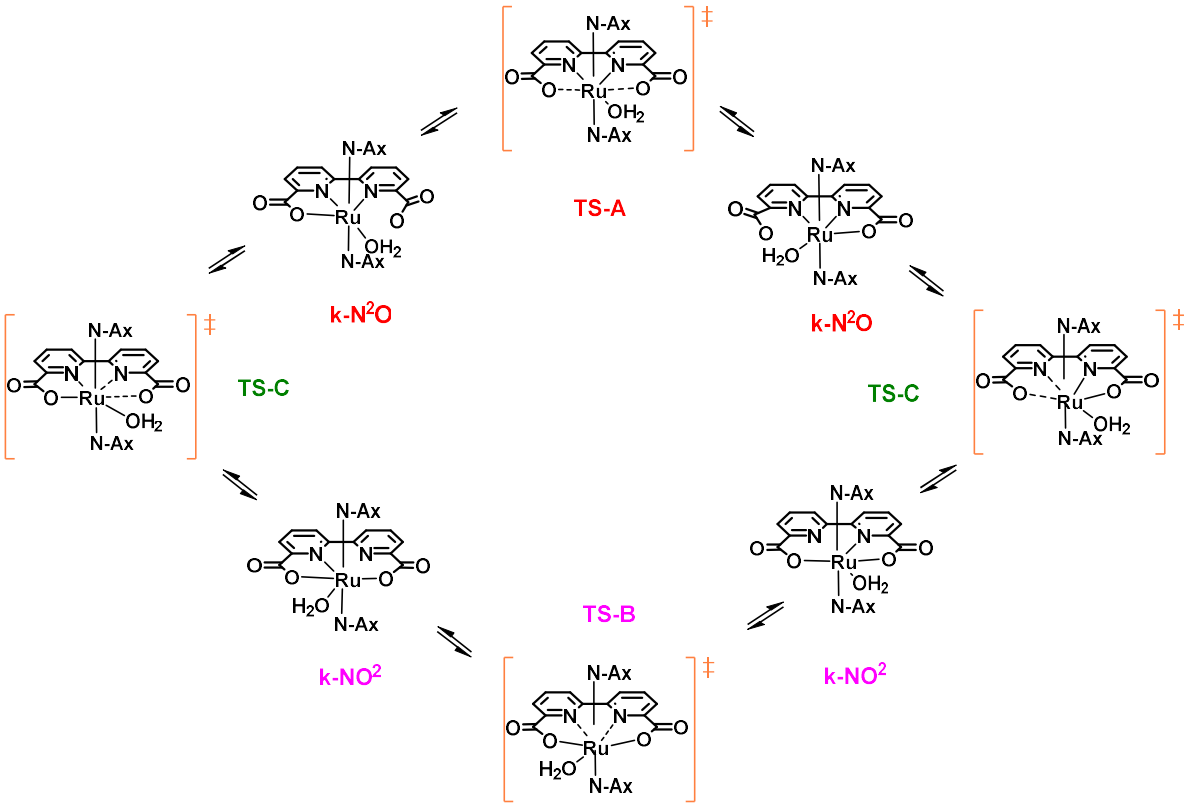

Figure 1. X-ray ORTEP plots (ellipsoids at 50% probability) and labeling scheme of **1** (left), the cationic part of $\mathbf{2}^{3+}$ (center) and **3** (right). Color codes: Ru, cyan; N, blue; O, red; C, black; H, light blue.

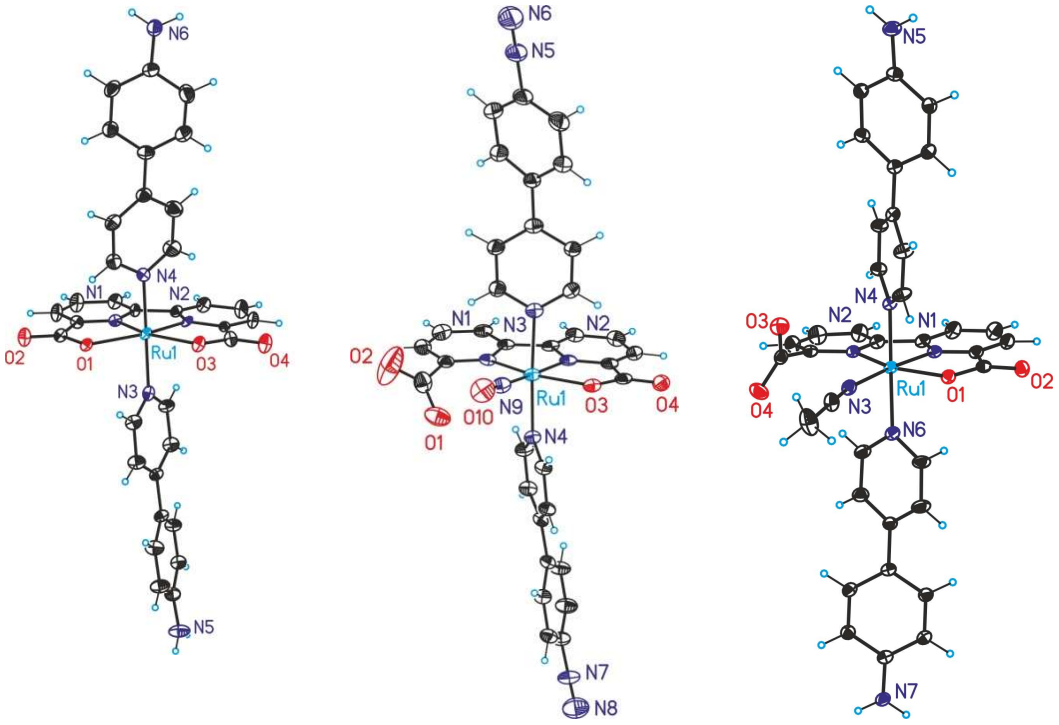

Figure 2. X-ray absorption spectroscopy analysis for **1** and $\mathbf{5^{3+}}$. Data for metallic Ru, RuO_2, and $[RuCl_3(trpy)]$ is shown for comparison. (A) Ru K-edge spectra. Inset: correlation between K-edge energies (determined at 50 % edge magnitude) and Ru oxidation states. (B) Fourier-transforms (FTs) of EXAFS spectra in the inset. FTs (experimental data) were calculated for k-values of 1.8-14.2 $Å^{-1}$ and using $\cos^2$ windows extending over 10 % at both k-range ends. Spectra were vertically shifted for comparison. Inset, EXAFS oscillations in k-space. Thin black lines are experimental data whereas colored lines are simulations using parameters shown in Table 1 and SI.

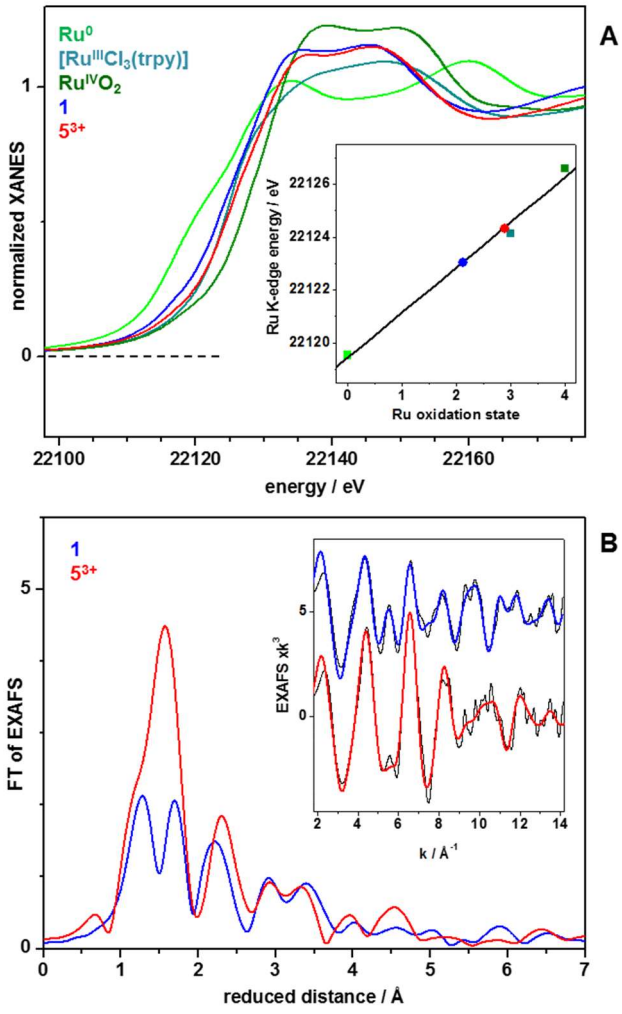

Figure 3. Ball and stick representation of the optimized structures at M06 level of theory for **[2-κ-N²O]³⁺** and the transition state **[2-κ-(NO)³]³⁺** that interconverts the two limiting structures shown in Scheme 2. Color code: Ru, cyan; C, gray; N, blue; O, red, H atoms of the ligands were omitted for clarity.

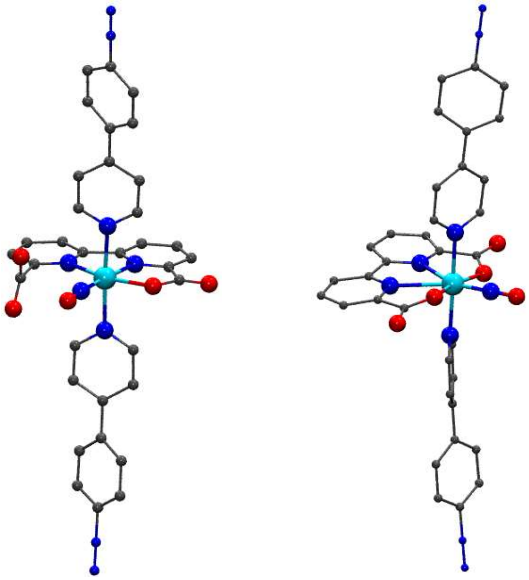

[2-κ-N²O]³⁺ **[2-κ-(NO)³]³⁺**

Figure 4. Left, VT -¹H-NMR spectra for **2³⁺** in acetone-d_6. Right, computed chemical shifts at M06 level of theory for the bda^{2-} hydrogens in **2³⁺**. See Chart 1 for the labeling.

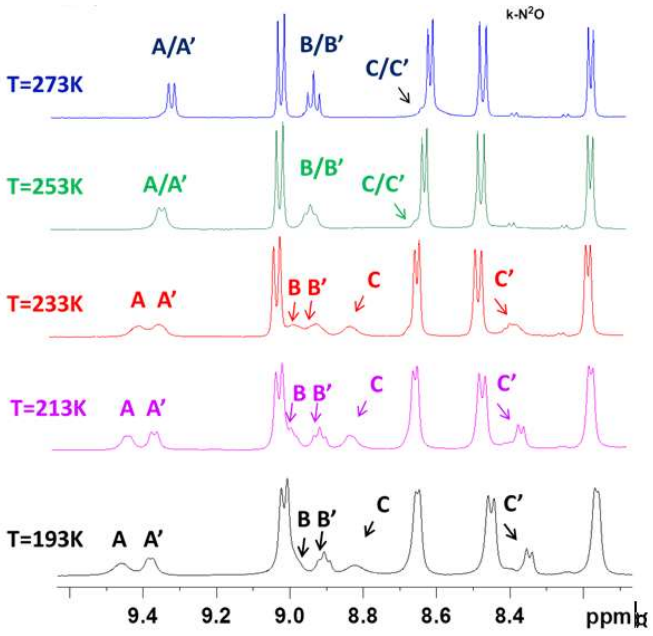

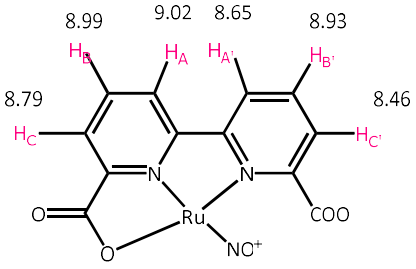

Figure 5. Left, ^{1}H-NMR of **1** in methanol-d_4 (cyan spectrum) and of $\mathbf{4}^{2+}$ with different amounts of a solution of 0.1 M CF_3SO_3D in D_2O (labeled as D_2O, pD = 1.0) at 298 K. Right, VT ^{1}H-NMR of $\mathbf{4}^{2+}$ in methanol-d_4 with 25% D_2O, pD = 1.0. Samples prepared under rigorous N_2 atmosphere. See Chart 1 for the labeling.

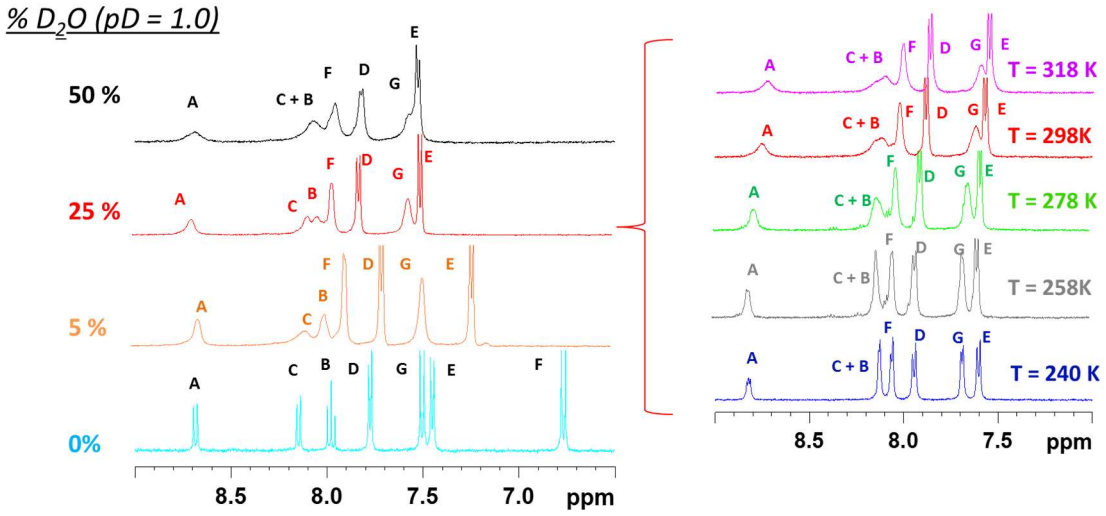

Figure 6. Ball and stick representation of the optimized structures of $\mathbf{[4\text{-}\kappa\text{-}N^2O(H_2O)_4]^{2+}}$, $\mathbf{[4\text{-}\kappa\text{-}NO^2(H_2O)_4]^{2+}}$, $\mathbf{[5\text{-}\kappa\text{-}N^2O(H_2O)_4]^{3+}}$ and $\mathbf{[5\text{-}\kappa\text{-}NO^2(H_2O)_4]^{3+}}$ at M06 level of theory. Dashed line indicates elongated bond. Color code: Ru, cyan; C, gray; N, blue; O, red, H atoms of the ligands were omitted for clarity.

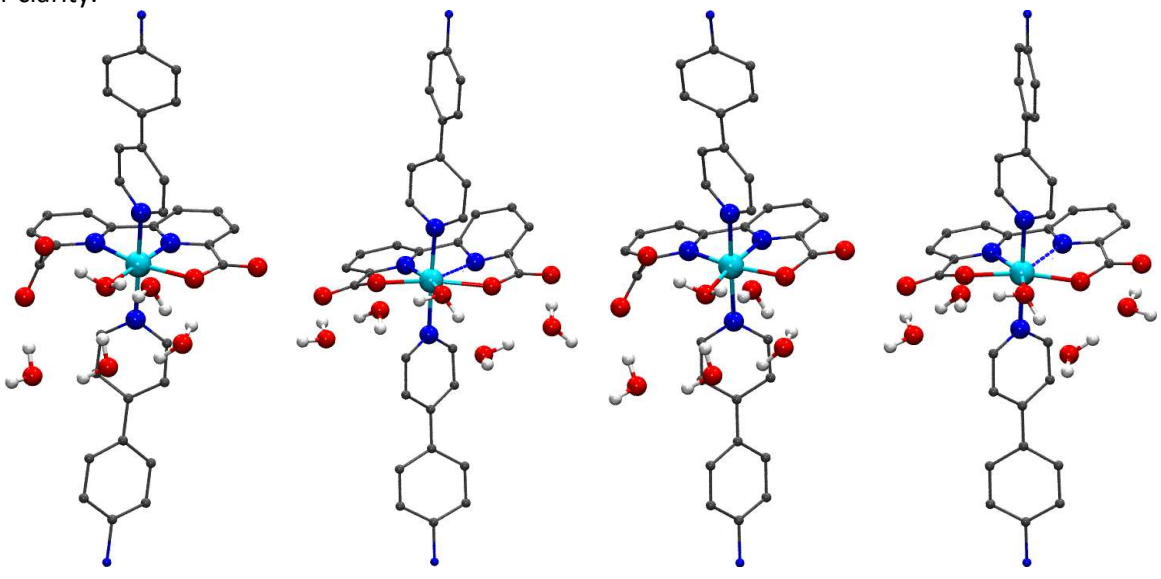

$\mathbf{[4\text{-}\kappa\text{-}N^2O(H_2O)_4]^{2+}}$ $\mathbf{[4\text{-}\kappa\text{-}NO^2(H_2O)_4]^{2+}}$ $\mathbf{[5\text{-}\kappa\text{-}N^2O(H_2O)_4]^{3+}}$ $\mathbf{[5\text{-}\kappa\text{-}NO^2(H_2O)_4]^{3+}}$

Graphical Abstract

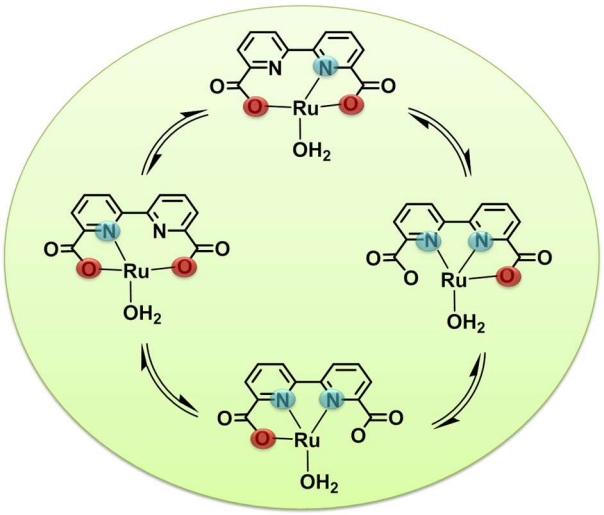

Lost & Found Coordination

Ru-bda catalysts are powerful water oxidation catalysts thanks to seven coordination provided by the ligand framework. While the hepta-coordination provides stability when the Ru complex reaches high oxidation states, the Ru center can only afford to coordinate 6 of these positions in the first catalytic steps. Herein, we study this coordination rearrangement by characterizing new Ru-bda complexes by several techniques including Variable temperature NMR, X-ray absorption spectroscopy and single-crystal XRD.

References

[1] S. W. Gersten, G. J. Samuels, T. J. J. Meyer, *J. Am. Chem. Soc.* **1982**, *104*, 4029–4030.

[2] P. Garrido-Barros, C. Gimbert-Surinach, R. Matheu, X. Sala, A. Llobet, *Chem. Soc. Rev.* **2017**, *46*, 6088-6098.

[3] I. López, M. Z. Ertem, S. Maji, J. Benet-Buchholz, A. Keidel, U. Kuhlmann, P. Hildebrandt, C. J. Cramer, V. S. Batista, A. Llobet, *Angew. Chem. Int. Ed.* **2014**, *53*, 205-209.

[4] J. Creus, R. Matheu, I. Peñafiel, D. Moonshiram, P. Blondeau, J. Benet-Buchholz, J. García-Antón, X. Sala, C. Godard, A. Llobet, *Angew. Chem. Int. Ed.* **2016**, *55*, 15382-15386.

[5] R. Matheu, I. A. Moreno-Hernandez, X. Sala, H. B. Gray, B. S. Brunschwig, A. Llobet, N. S. Lewis, *J. Am. Chem. Soc.* **2017**, *139*, 11345-11348.

[6] L. Duan, F. Bozoglian, S. Mandal, B. Stewart, T. Privalov, A. Llobet, L. Sun, *Nat. Chem.* **2012**, *4*, 418-423.

[7] C. J. Richmond, R. Matheu, A. Poater, L. Falivene, J. Benet-Buchholz, X. Sala, L. Cavallo, A. Llobet, *Chem. Eur. J.* **2014**, *20*, 17282–17286.

[8] L. Wang, L. Duan, Y. Wang, M. S. G. Ahlquist, L. Sun, *Chem. Commun.* **2014**, *50*, 12947-12950.

[9] M. Schulze, V. Kunz, P. D. Frischmann, F. Würthner, *Nat. Chem.* **2016***, 8,* 576-583.

[10] F. Li, B. Zhang, X. Li, Y. Jiang, L. Chen, Y. Li, L. Sun, *Angew. Chem. Int. Ed.* **2011**, *50*, 12276-12279

[11] H. Dau, M. Haumann, *Biochim. Biophys. Acta* **2007**, *1767*, 472-483.

[12] N. Cox, M. Retegan, F. Neese, D. A. Pantazis, A. Boussac, W. Lubitz, *Science* **2014**, *345*, 804-808.

[13] R. Matheu, M. Z. Ertem, J. Benet-Buchholz, E. Coronado, V. S. Batista, X. Sala, A. Llobet, *J. Am. Chem. Soc.* **2015**, *137,* 10786-10795.

[14] R. Matheu, M. Z. Ertem, M. Pipelier, J. Lebreton, D. Dubreuil, J. Benet-Buchholz, X. Sala, A. Tessier, A. Llobet, *ACS Catal.* **2018**, *8*, *2039–2048.*

[15] L. Duan, L. Wang, F. Li, F. Li, L. Sun, *Acc. Chem. Res.* **2015**, *48*, 2084-2096.

[16] L. Duan, L. Wang, F. A. K. Inge, A. Fischer, X. Zou, L. Sun, *Inorg. Chem.* **2013**, *52*, 7844-7852

[17] R. Matheu, L. Francàs, P. Chernev, M. Z. Ertem, V. S. Batista, M. Haumann, X. Sala, A. Llobet, *ACS Catal.* **2015**, *5*, 3422-3429.

[18] Y. Gao, X. Ding, J. Liu, L. Wang, Z. Lu, L. Li, L. Sun, *J. Am. Chem. Soc.* **2013**, *135*, 4219-4222.

[19] F. Li, B. Zhang, X. Li, Y. Jiang, L. Chen, Y. Li, L. Sun, *Angew. Chem., Int. Ed.* **2011**, *50*, 12276-12279.

[20] J. J. Concepcion, D. K. Zhong, D. J. Szalda, J. T. Muckerman, E. Fujita, *Chem. Commun.* **2015**, *51*, 4105-4108.

[21] M. V. Sheridan, B. D. Sherman, R. L. Coppo, D. Wang, S. L. Marquard, K.-R. Wee, N. Y. Murakami Iha, T. J. Meyer, *ACS Energy Lett.* **2016**, *1*, 231-236.

[22] X. Sala, S. Maji, R. Bofill, J. Garcia-Anton, L. Escriche, A. Llobet, *Acc. Chem. Res*. **2014**, *47*, 504-516.

[23] Q. Daniel, P. Huang, T. Fan, Y. Wang, L. Duan, L. Wang, F. Li, Z. Rinkevicius, F. Mamedov, M. S. G. Ahlquist, S. Styring, L. Sun, *Coord. Chem. Rev.* **2017**, *346*, 206-215.

[24] L. Duan, A. Fischer, Y. Xu, L. Sun, *J. Am. Chem. Soc.* **2009**, *131*, 10397-10399.

[25] P. Pyykkö, *J. Organomet. Chem.* **2006**, *691*, 4336-4340.

[26] J. Nyhlén, L. Duan, B. Åkermark, L. Sun, T. Privalov, *Angew. Chem. Int. Ed.* **2010**, *49*, 1773-1777.

[27] D. W.Stephan, *Comp. Inorg. Chem. II.* Eds: Reedijk, J.; Poeppelmeier, K. Elsevier, Oxford, April **2013**.

[28] P. P. Samuel, K. C. Mondal, N. Amin Sk, H. W. Roesky, E. Carl, R. Neufeld, D. Stalke, S. Demeshko, F. Meyer, L. Ungur, L. F. Chibotaru, J. Christian, V. Ramachandran, J. van Tol, N. S. Dalal, *J. Am. Chem. Soc.* **2014**, *136*, 11964-11971.

[29] C. Di Giovanni, A. Poater, J. Benet-Buchholz, L. Cavallo, M. Sola, A. Llobet, *Chem. Eur. J*. **2014**, *20*, 3898-3902.

[30]I. Romero, M. Rodríguez, A. Llobet, M.-N. Collomb-Dunand-Sauthier, A. Deronzier, T. Parella, H. Stoeckli-Evans, *J. Chem. Soc., Dalton Trans*. **2000**, 1689-1694.

[31] C. Di Giovanni, L. Vaquer, X. Sala, J. Benet-Buchholz, A. Llobet, *Inorg. Chem.* **2013**, *52*, 4335-4345.

[32] Y. Zhao, D. Truhlar, *Theor. Chem. Acc*. **2008**, *120*, 215-241.

[33] J. Pinson, F. Podvorica, *Chem. Soc. Rev.* **2005**, *34*, 429-439.

[34] L. Tong, L. Duan, Y. Xu, T. Privalov, L. Sun, *Angew. Chem. Int. Ed.* **2011**, *50*, 445-449.

[35] L. Alibabaei, B. D. Sherman, M. R. Norris, M. K. Brennaman, T. J. Meyer, *Proc. Natl. Acad. Sci. U.S.A.* **2015**, *112*, 5899-5902.

[36] R. G. Pearson, *J. Am. Chem. Soc.* **1963***, 85,* 3533-3539.

[37] H. C. Stynes, J. A. Ibers, *Inorg. Chem.* **1971**, *10*, 2304-2308.